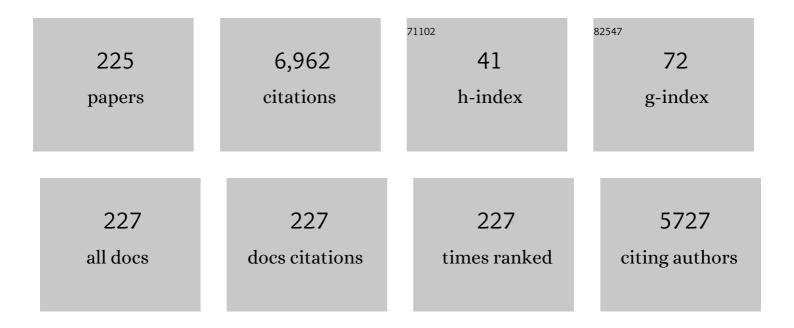
List of Publications by Year in descending order

Source: https://exaly.com/author-pdf/1388064/publications.pdf Version: 2024-02-01



IED-REN YANG

#	Article	IF	CITATIONS
1	Aging reactions in a 17-4 PH stainless steel. Materials Chemistry and Physics, 2002, 74, 134-142.	4.0	317
2	The effect of high-temperature exposure on the microstructural stability and toughness property in a 2205 duplex stainless steel. Materials Science & Engineering A: Structural Materials: Properties, Microstructure and Processing, 2002, 338, 259-270.	5.6	292
3	Effects of solution treatment and continuous cooling on Ï <i>f</i> -phase precipitation in a 2205 duplex stainless steel. Materials Science & Engineering A: Structural Materials: Properties, Microstructure and Processing, 2001, 311, 28-41.	5.6	254
4	Interphase precipitation of nanometer-sized carbides in a titanium–molybdenum-bearing low-carbon steel. Acta Materialia, 2011, 59, 6264-6274.	7.9	254
5	Precipitation hardening of high-strength low-alloy steels by nanometer-sized carbides. Materials Science & Engineering A: Structural Materials: Properties, Microstructure and Processing, 2009, 499, 162-166.	5.6	202
6	Mechanical stabilisation of austenite. Materials Science and Technology, 2006, 22, 641-644.	1.6	194
7	Retarded phase transition by fluorine doping in Li-rich layered Li 1.2 Mn 0.54 Ni 0.13 Co 0.13 O 2 cathode material. Journal of Power Sources, 2015, 283, 162-170.	7.8	190
8	Transmission electron microscopy investigation of separated nucleation and in-situ nucleation in AA7050 aluminium alloy. Acta Materialia, 2018, 149, 377-387.	7.9	168
9	The low-temperature aging embrittlement in a 2205 duplex stainless steel. Materials Science & Engineering A: Structural Materials: Properties, Microstructure and Processing, 2004, 379, 119-132.	5.6	141
10	Structure and formation mechanism of V defects in multiple InGaNâ^•GaN quantum well layers. Journal of Applied Physics, 2006, 99, 073505.	2.5	124
11	Quantum Confinement Effect in Diamond Nanocrystals Studied by X-Ray-Absorption Spectroscopy. Physical Review Letters, 1999, 82, 5377-5380.	7.8	118
12	Stabilization of retained austenite by the two-step intercritical heat treatment and its effect on the toughness of a low alloyed steel. Materials & Design, 2014, 59, 193-198.	5.1	111
13	An atomic scale structural investigation of nanometre-sized ηÂprecipitates in the 7050 aluminium alloy. Acta Materialia, 2019, 174, 351-368.	7.9	110
14	Microstructural characterization of simulated heat affected zone in a nitrogen-containing 2205 duplex stainless steel. Materials Science & Engineering A: Structural Materials: Properties, Microstructure and Processing, 2002, 338, 166-181.	5.6	104
15	Characterization of interphase-precipitated nanometer-sized carbides in a Ti–Mo-bearing steel. Scripta Materialia, 2009, 61, 616-619.	5.2	103
16	Stability of retained austenite in multi-phase microstructure during austempering and its effect on the ductility of a low carbon steel. Materials Science & Engineering A: Structural Materials: Properties, Microstructure and Processing, 2014, 603, 69-75.	5.6	100
17	A unified constitutive model for asymmetric tension and compression creep-ageing behaviour of naturally aged Al-Cu-Li alloy. International Journal of Plasticity, 2017, 89, 130-149.	8.8	100
18	Phase transformation in AISI 410 stainless steel. Materials Science & Engineering A: Structural Materials: Properties, Microstructure and Processing, 2002, 332, 1-10.	5.6	92

#	Article	IF	CITATIONS
19	Interactions between deformation-induced defects and carbides in a vanadium-containing TWIP steel. Scripta Materialia, 2012, 66, 1018-1023.	5.2	89
20	Orientation relationship transition of nanometre sized interphase precipitated TiC carbides in Ti bearing steel. Materials Science and Technology, 2010, 26, 421-430.	1.6	73
21	The effect of compressive deformation of austenite on the bainitic ferrite transformation in Feî—,Mnî—,Siî—,C steels. Materials Science & Engineering A: Structural Materials: Properties, Microstructure and Processing, 2000, 278, 278-291.	5.6	68
22	Complementary use of transmission electron microscopy and atom probe tomography for the examination of plastic accommodation in nanocrystalline bainitic steels. Acta Materialia, 2011, 59, 6117-6123.	7.9	68
23	Formation and structure of inverted hexagonal pyramid defects in multiple quantum wells InGaN/GaN. Applied Physics Letters, 2003, 82, 718-720.	3.3	66
24	Interplay of Three-Dimensional Morphologies and Photocarrier Dynamics of Polymer/TiO2Bulk Heterojunction Solar Cells. Journal of the American Chemical Society, 2011, 133, 11614-11620.	13.7	66
25	Phase quantification in low carbon Nb-Mo bearing steel by electron backscatter diffraction technique coupled with kernel average misorientation. Materials Characterization, 2018, 139, 49-58.	4.4	61
26	Nanostructures and carrier localization behaviors of green-luminescence InGaN/GaN quantum-well structures of various silicon-doping conditions. Applied Physics Letters, 2004, 84, 2506-2508.	3.3	59
27	The effect of finish rolling temperature and tempering on the microstructure, mechanical properties and dislocation density of direct-quenched steel. Materials Characterization, 2018, 139, 1-10.	4.4	58
28	Orientation relationships between adjacent plates of acicular ferrite in steel weld deposits. Materials Science and Technology, 1989, 5, 93-97.	1.6	52
29	Ultralow threading dislocation density in GaN epilayer on near-strain-free GaN compliant buffer layer and its applications in hetero-epitaxial LEDs. Scientific Reports, 2015, 5, 13671.	3.3	51
30	Effects of chemical composition, rolling and cooling conditions on the amount of martensite/austenite (M/A) constituent formation in low carbon bainitic steels. Materials Science & Engineering A: Structural Materials: Properties, Microstructure and Processing, 1992, 154, 43-49.	5.6	50
31	Microstructures and fatigue crack growth of EH36 TMCP steel weldments. International Journal of Fatigue, 1999, 21, 857-864.	5.7	49
32	Atomic-scale strain field and In atom distribution in multiple quantum wells InGaN/GaN. Applied Physics Letters, 2003, 82, 715-717.	3.3	48
33	Gamma (γ) phase transformation in pulsed GTAW weld metal of duplex stainless steel. Materials Science & Engineering A: Structural Materials: Properties, Microstructure and Processing, 2006, 420, 26-33.	5.6	48
34	Formation polarity dependent improved resistive switching memory characteristics using nanoscale (1.3 nm) core-shell IrOx nano-dots. Nanoscale Research Letters, 2012, 7, 194.	5.7	48
35	Tensile Response of Two Nanoscale Bainite Composite-Like Structures. Jom, 2015, 67, 2223-2235.	1.9	48
36	Solution processable nanocarbon platform for polymer solar cells. Energy and Environmental Science, 2011, 4, 3521.	30.8	47

#	Article	IF	CITATIONS
37	Structure and properties of hot-pressed lead-free (Ba0.85Ca0.15)(Zr0.1Ti0.9)O3 piezoelectric ceramics. RSC Advances, 2013, 3, 20693.	3.6	47
38	Influence of welding pass on microstructure and toughness in the reheated zone of multi-pass weld metal of 550 MPa offshore engineering steel. Materials Science & Engineering A: Structural Materials: Properties, Microstructure and Processing, 2017, 702, 196-205.	5.6	47
39	ZnO-based ultra-violet light emitting diodes and nanostructures fabricated by atomic layer deposition. Semiconductor Science and Technology, 2012, 27, 074005.	2.0	46
40	Microstructural evolutions of low carbon Nb/Mo-containing bainitic steels during high-temperature tempering. Materials Characterization, 2017, 131, 298-305.	4.4	46
41	Acicular ferrite transformation in alloy-steel weld metals. Journal of Materials Science, 1991, 26, 839-845.	3.7	44
42	Mechanical Stabilization of Austenite against Bainitic Reaction in Fe–Mn–Si–C Bainitic Steel. Materials Transactions, JIM, 1996, 37, 579-585.	0.9	44
43	lsothermal treatment influence on nanometer-size carbide precipitation of titanium-bearing low carbon steel. Materials Letters, 2011, 65, 396-399.	2.6	44
44	Growth of highly transparent nanocrystalline diamond films and a spectroscopic study of the growth. Journal of Applied Physics, 2001, 89, 753-759.	2.5	43
45	High-entropy CoCrFeMnNi alloy subjected to high-strain-rate compressive deformation. Materials Characterization, 2019, 147, 193-198.	4.4	43
46	Negative voltage modulated multi-level resistive switching by using a Cr/BaTiOx/TiN structure and quantum conductance through evidence of H2O2 sensing mechanism. Scientific Reports, 2017, 7, 4735.	3.3	42
47	The effect of prior compressive deformation of austenite on toughness property in an ultra-low carbon bainitic steel. Materials Chemistry and Physics, 2001, 69, 113-124.	4.0	41
48	Charge storage characteristics of atomic layer deposited RuOx nanocrystals. Applied Physics Letters, 2007, 90, 253108.	3.3	41
49	Conductive and transparent multilayer films for low-temperature TiO2/Ag/SiO2 electrodes by E-beam evaporation with IAD. Nanoscale Research Letters, 2014, 9, 35.	5.7	41
50	Effect of interpass temperature on the microstructure and mechanical properties of multi-pass weld metal in a 550-MPa-grade offshore engineering steel. Welding in the World, Le Soudage Dans Le Monde, 2017, 61, 1155-1168.	2.5	41
51	Low-cycle fatigue-induced martensitic transformation in SAF 2205 duplex stainless steel. Materials Science & Engineering A: Structural Materials: Properties, Microstructure and Processing, 2005, 398, 349-359.	5.6	40
52	Microstructural characterization and strengthening behavior of nanometer sized carbides in Ti–Mo microalloyed steels during continuous cooling process. Materials Characterization, 2016, 114, 18-29.	4.4	40
53	Effects of interphase TiC precipitates on tensile properties and dislocation structures in a dual phase steel. Materials Characterization, 2017, 123, 153-158.	4.4	40
54	Characterisation of severely deformed austenitic stainless steel wire. Materials Science and Technology, 2005, 21, 1323-1328.	1.6	39

#	Article	IF	CITATIONS
55	Inverse effect of strain rate on mechanical behavior and phase transformation of superaustenitic stainless steel. Scripta Materialia, 2007, 56, 717-720.	5.2	38
56	High energy spinel-structured cathode stabilized by layered materials for advanced lithium-ion batteries. Journal of Power Sources, 2014, 271, 604-613.	7.8	37
57	Microstructural characterization of Charpy-impact-tested nanostructured bainite. Materials Characterization, 2015, 107, 63-69.	4.4	37
58	Continuous heating transformation of bainite to austenite. Materials Science & Engineering A: Structural Materials: Properties, Microstructure and Processing, 1991, 131, 99-113.	5.6	36
59	Influence of acicular ferrite and bainite microstructures on toughness for an ultra-low-carbon alloy steel weld metal. Journal of Materials Science Letters, 1993, 12, 1290-1293.	0.5	36
60	Ultraviolet Electroluminescence From n-ZnO–SiO\$_{2}\$–ZnO Nanocomposite/p-GaN Heterojunction Light-Emitting Diodes at Forward and Reverse Bias. IEEE Photonics Technology Letters, 2008, 20, 1772-1774.	2.5	36
61	NH4F surface modification of Li-rich layered cathode materials. Solid State Ionics, 2014, 264, 36-44.	2.7	35
62	Improved resistive switching phenomena and mechanism using Cu-Al alloy in a new Cu:AlOx/TaOx/TiN structure. Journal of Alloys and Compounds, 2015, 637, 517-523.	5.5	35
63	UV Electroluminescence and Structure of n-ZnO/p-GaN Heterojunction LEDs Grown by Atomic Layer Deposition. IEEE Journal of Quantum Electronics, 2010, 46, 265-271.	1.9	34
64	In-situ transmission electron microscopy investigation of the deformation behavior of spinodal nanostructured Î-ferrite in a duplex stainless steel. Scripta Materialia, 2016, 125, 44-48.	5.2	34
65	White-Light Electroluminescence From n-ZnO/p-GaN Heterojunction Light-Emitting Diodes at Reverse Breakdown Bias. IEEE Transactions on Electron Devices, 2011, 58, 3970-3975.	3.0	33
66	ZnO-based heterojunction light-emitting diodes on p-SiC(4H) grown by atomic layer deposition. Applied Physics B: Lasers and Optics, 2010, 98, 767-772.	2.2	32
67	Low-alloy duplex, directly quenched transformation-induced plasticity steel. Scripta Materialia, 2011, 65, 604-607.	5.2	32
68	Microstructural examination of 2.25Crî—,1Mo Steel Steam pipes after extended service. Materials Characterization, 1993, 30, 75-88.	4.4	31
69	Highly transparent nano-crystalline diamond films via substrate pretreatment and methane fraction optimization. Thin Solid Films, 1998, 332, 34-39.	1.8	30
70	Enhanced resistive switching phenomena using low-positive-voltage format and self-compliance IrO x /GdO x /W cross-point memories. Nanoscale Research Letters, 2014, 9, 12.	5.7	30
71	Effect of Compressive Deformation on the Transformation Behavior of an Ultra-Low-Carbon Bainitic Steel. Materials Transactions, JIM, 1993, 34, 658-668.	0.9	29
72	The transition from interphase-precipitated carbides to fibrous carbides in a vanadium-containing medium-carbon steel. Scripta Materialia, 2013, 68, 829-832.	5.2	29

#	Article	IF	CITATIONS
73	Optical and structural properties of InGaN/GaN multiple quantum well structure grown by metalorganic chemical vapor deposition. Thin Solid Films, 2006, 498, 123-127.	1.8	28
74	Secondary hardened bainite. Materials Science and Technology, 2014, 30, 1014-1023.	1.6	28
75	Strain rate dependence on the evolution of microstructure and deformation mechanism during nanoscale deformation in low carbon-high Mn TWIP steel. Materials Science & Engineering A: Structural Materials: Properties, Microstructure and Processing, 2019, 742, 116-123.	5.6	28
76	Substructures of martensite in Fe–1C–17Cr stainless steel. Scripta Materialia, 2010, 62, 670-673.	5.2	27
77	Effect of Cr and Al additions on the development of interphase-precipitated carbides strengthened dual-phase Ti-bearing steels. Materials and Design, 2017, 119, 319-325.	7.0	27
78	Evolution of resistive switching mechanism through H 2 O 2 sensing by using TaO x -based material in W/Al 2 O 3 /TaO x /TiN structure. Applied Surface Science, 2018, 433, 51-59.	6.1	27
79	The development of ultra-low-carbon bainitic steels. Materials & Design, 1992, 13, 335-338.	5.1	26
80	The Influence of Plastic Deformation and Cooling Rates on the Microstructural Constituents of an Ultra-low Carbon Bainitic Steel ISIJ International, 1995, 35, 1013-1019.	1.4	26
81	Growth, characterization, optical and X-ray absorption studies of nano-crystalline diamond films. Diamond and Related Materials, 2000, 9, 877-882.	3.9	25
82	Effect of Boron on the Strength and Toughness of Direct-Quenched Low-Carbon Niobium Bearing Ultra-High-Strength Martensitic Steel. Metallurgical and Materials Transactions A: Physical Metallurgy and Materials Science, 2017, 48, 5344-5356.	2.2	25
83	The effects of rolling processes on the microstructure and mechanical properties of ultralow carbon bainitic steels. Materials Science & Engineering A: Structural Materials: Properties, Microstructure and Processing, 1992, 157, 29-36.	5.6	24
84	The effect of stress on the Widmanstäten ferrite transformation. Materials Science & Engineering A: Structural Materials: Properties, Microstructure and Processing, 1997, 223, 158-167.	5.6	24
85	Mechanical behavior and microstructural evolution of nanostructured bainite under high-strain rate deformation by Hopkinson bar. Scripta Materialia, 2016, 115, 46-51.	5.2	23
86	Densification, microstructure evolution, and microwave dielectric properties of Mg 1-x Ca x ZrTa 2 O 8 ceramics. Journal of the European Ceramic Society, 2017, 37, 2825-2831.	5.7	23
87	Effects of substrate pretreatment and methane fraction on the optical transparency of nanocrystalline diamond thin films. Journal of Materials Research, 1998, 13, 1769-1773.	2.6	22
88	Direct determination of atomic structure in multiple quantum wells InGaN/GaN. Applied Physics Letters, 2002, 80, 761-762.	3.3	22
89	Sympathetic nucleation of austenite in a Fe–22Cr–5Ni duplex stainless steel. Scripta Materialia, 2007, 56, 673-676.	5.2	22
90	Cyclic deformation and phase transformation of 6Mo superaustenitic stainless steel. Metals and Materials International, 2007, 13, 275-283.	3.4	22

#	Article	IF	CITATIONS
91	Dynamic strain aging in low cycle fatigue of duplex titanium alloys. Materials Science & Engineering A: Structural Materials: Properties, Microstructure and Processing, 2011, 528, 4381-4389.	5.6	22
92	Superledge Model for Interphase Precipitation During Austenite-to-Ferrite Transformation. Metallurgical and Materials Transactions A: Physical Metallurgy and Materials Science, 2014, 45, 5351-5361.	2.2	22
93	Microstructure and mechanical behaviors of GPa-grade TRIP steels enabled by hot-rolling processes. Materials Science & Engineering A: Structural Materials: Properties, Microstructure and Processing, 2019, 761, 138005.	5.6	22
94	HR-STEM investigation of atomic lattice defects in different types of Î∙ precipitates in creep-age forming Al–Zn–Mg–Cu aluminium alloy. Materials Science & Engineering A: Structural Materials: Properties, Microstructure and Processing, 2021, 815, 141213.	5.6	22
95	Suppression of phase separation in InGaN layers grown on lattice-matched ZnO substrates. Journal of Crystal Growth, 2009, 311, 4628-4631.	1.5	21
96	The effect of compressive deformation of austenite on the WidmanstÃ æ en ferrite transformation in Fe–Mn–Si–C steel. Materials Science & Engineering A: Structural Materials: Properties, Microstructure and Processing, 1999, 264, 139-150.	5.6	20
97	The effect of strain ratio on morphology of dislocation in low cycle fatigued SAF 2205 DSS. Materials Chemistry and Physics, 2006, 98, 103-110.	4.0	19
98	Structure and stimulated emission of a high-quality zinc oxide epilayer grown by atomic layer deposition on the sapphire substrate. Thin Solid Films, 2010, 519, 536-540.	1.8	19
99	Cross-Point Resistive Switching Memory and Urea Sensing by Using Annealed GdO _x Film in IrO _x /GdO _x /W Structure for Biomedical Applications. Journal of the Electrochemical Society, 2017, 164, B127-B135.	2.9	19
100	Crystallographic examination of the interaction between texture evolution, mechanically induced martensitic transformation and twinning in nanostructured bainite. Journal of Alloys and Compounds, 2018, 752, 505-519.	5.5	19
101	Microstructural degeneration of simulated heat-affected zone in 2.25Cr–1Mo steel during high-temperature exposure. Materials Science & Engineering A: Structural Materials: Properties, Microstructure and Processing, 2003, 340, 15-32.	5.6	18
102	Microtwin formation in the α phase of duplex titanium alloys affected by strain rate. Materials Science & Engineering A: Structural Materials: Properties, Microstructure and Processing, 2011, 528, 2271-2276.	5.6	18
103	Three phase crystallography and solute distribution analysis during residual austenite decomposition in tempered nanocrystalline bainitic steels. Materials Characterization, 2014, 88, 15-20.	4.4	18
104	Martensitic transformations in AISI 440C stainless steel. Materials Science & Engineering A: Structural Materials: Properties, Microstructure and Processing, 2006, 438-440, 276-280.	5.6	17
105	Structure and Electro-Optical Properties of Thin Films Grown by Alternate Atomic Layer Deposition of ZnO and Al ₂ O ₃ on the Sapphire Substrate. Materials Transactions, 2010, 51, 219-226.	1.2	17
106	Highly Reliable Label-Free Detection of Urea/Glucose and Sensing Mechanism Using SiO2and CdSe-ZnS Nanoparticles in Electrolyte-Insulator-Semiconductor Structure. Journal of the Electrochemical Society, 2016, 163, B580-B587.	2.9	17
107	Microstructural mechanisms controlling the mechanical behaviour of ultrafine grained martensite/austenite microstructures in a metastable stainless steel. Materials and Design, 2019, 181, 107922.	7.0	17
108	Electron work function: an indicative parameter towards a novel material design methodology. Scientific Reports, 2021, 11, 11565.	3.3	17

#	Article	IF	CITATIONS
109	Reaustenitization experiments on some high-strength steel weld deposits. Materials Science & Engineering A: Structural Materials: Properties, Microstructure and Processing, 1989, 118, 155-170.	5.6	16
110	Improvements of InGaNâ^•GaN quantum-well interfaces and radiative efficiency with InN interfacial layers. Applied Physics Letters, 2004, 84, 5422-5424.	3.3	16
111	Synergistic effect of austenitizing temperature and hot plastic deformation strain on the precipitation behavior in novel HSLA steel. Materials Science & Engineering A: Structural Materials: Properties, Microstructure and Processing, 2015, 639, 145-154.	5.6	16
112	Highly transparent nano-crystalline diamond films grown by microwave CVD. Solid State Communications, 1998, 107, 301-305.	1.9	15
113	Study of carrier localization in InGaN/GaN quantum well blue-light-emitting diode structures. Journal of Crystal Growth, 2006, 287, 354-358.	1.5	15
114	Structural and compositional analyses of a strained AlGaNâ^•GaN superlattice. Journal of Applied Physics, 2006, 100, 013110.	2.5	15
115	ZnO quantum dots embedded in a SiO ₂ nanoparticle layer grown by atomic layer deposition. Physica Status Solidi - Rapid Research Letters, 2009, 3, 88-90.	2.4	15
116	An efficient Si light-emitting diode based on an n- ZnO/SiO ₂ –Si nanocrystals-SiO ₂ /p-Si heterostructure. Nanotechnology, 2009, 20, 445202.	2.6	15
117	Characterization of nano-sized precipitation and dislocations and the correlation with mechanical properties of a low alloy TRIP-aided steel. Materials Science & amp; Engineering A: Structural Materials: Properties, Microstructure and Processing, 2019, 763, 138149.	5.6	15
118	Molybdenum alloying in high-performance flat-rolled steel grades. Advances in Manufacturing, 2020, 8, 15-34.	6.1	15
119	Effects of silicon doping on the nanostructures of InGaN/GaN quantum wells. Journal of Crystal Growth, 2005, 279, 55-64.	1.5	14
120	Observation of V Defects in Multiple InGaN/GaN Quantum Well Layers. Materials Transactions, 2007, 48, 894-898.	1.2	14
121	Morphological evolution of GP zones and nanometer-sized precipitates in the AA2050 aluminium alloy. International Journal of Lightweight Materials and Manufacture, 2018, 1, 142-156.	2.1	14
122	Microstructural and electrical properties of epitaxial PtSi/p‣i(100) coâ€deposited under ultrahigh vacuum. Journal of Applied Physics, 1993, 74, 6251-6255.	2.5	13
123	Optical and structural studies of dual wavelength InGaN/GaN tunnel-injection light emitting diodes grown by metalorganic chemical vapor deposition. Thin Solid Films, 2013, 529, 269-274.	1.8	13
124	Crystallographic analysis of lenticular martensite in Fe–1.0C–17Cr stainless steel by electron backscatter diffraction. Materials Characterization, 2016, 113, 17-25.	4.4	13
125	Microstructure characterization and strengthening behavior of dual precipitation particles in Cu Ti microalloyed dual-phase steels. Materials and Design, 2019, 166, 107613.	7.0	13
126	Investigation on the ballistic induced nanotwinning in the Mn-free Fe27Co24Ni23Cr26 high entropy alloy plate. Materials Chemistry and Physics, 2021, 270, 124707.	4.0	13

#	Article	IF	CITATIONS
127	Mapping of multiple-quantum-well layers and structure of V defects in InGaN/GaN diodes. Applied Physics Letters, 2004, 84, 2271-2273.	3.3	12
128	A Transmission Electron Microscopy Observation of Dislocations in GaN Grown on (0001) Sapphire by Metal Organic Chemical Vapor Deposition. Japanese Journal of Applied Physics, 2008, 47, 7998.	1.5	12
129	Structure and Ultraviolet Electroluminescence of \$n hbox{-ZnO/SiO}_{2}hbox{-ZnO}\$ Nanocomposite/\$p\$ -GaN Heterostructure Light-Emitting Diodes. IEEE Transactions on Electron Devices, 2010, 57, 2195-2202.	3.0	12
130	Structural investigation of ZnO:Al films deposited on the Si substrates by radio frequency magnetron sputtering. Thin Solid Films, 2013, 545, 183-187.	1.8	12
131	Structural analysis of Au/TiO2 thin films deposited on the glass substrate. Applied Physics Letters, 2013, 102, .	3.3	12
132	Atomic-resolution energy dispersive X-ray spectroscopy mapping of η precipitates in an Al-Mg-Zn-Cu alloy. Materials Characterization, 2020, 166, 110448.	4.4	12
133	Microstrain and boundary misorientation evolution for recrystallized super DSS after deformation. Materials Chemistry and Physics, 2020, 246, 122815.	4.0	12
134	Dual ferrite-martensite treatments of a high-strength low-alloy ASTM A588 steel. Journal of Materials Science, 1991, 26, 889-898.	3.7	11
135	HfO2/HfAlO/HfO2Nanolaminate Charge Trapping Layers for High-Performance Nonvolatile Memory Device Applications. Japanese Journal of Applied Physics, 2007, 46, 1803-1807.	1.5	11
136	Simulated heat affected zone in ASTM A533-B steel plates under low heat inputs. Materials Chemistry and Physics, 2009, 117, 471-477.	4.0	11
137	Cross-sectional observation of the intermetallic phase in a galvannealed steel. Materials Science & Engineering A: Structural Materials: Properties, Microstructure and Processing, 2009, 499, 45-48.	5.6	11
138	Fabrication of ZnO Nanopillars by Atomic Layer Deposition. Materials Transactions, 2010, 51, 253-255.	1.2	11
139	P-Type ZnO:P Films Fabricated by Atomic Layer Deposition and Thermal Processing. Journal of the Electrochemical Society, 2011, 158, H516.	2.9	11
140	Precipitation behavior in bimodal ferrite grains in a low carbon Ti-V-bearing steel. Scripta Materialia, 2018, 143, 103-107.	5.2	11
141	A novel technique for developing a dual-phase steel with a lower strength difference between ferrite and martensite. Materials Today Communications, 2020, 23, 100895.	1.9	11
142	Investigation of nanotwins in the bimodal-structured Fe22Co22Ni20Cr22Mn14 alloy subjected to high-strain-rate deformation at cryogenic temperatures. Materials Characterization, 2020, 170, 110667.	4.4	11
143	Metallurgical Effects of Niobium in Dual Phase Steel. Metals, 2020, 10, 504.	2.3	11
144	Age Hardening in Martensitic/Bainitic Matrices in a Copper-Bearing Steel. Materials Transactions, JIM, 2000, 41, 1312-1321.	0.9	10

#	Article	IF	CITATIONS
145	Title is missing!. Journal of Materials Science, 2003, 38, 2373-2391.	3.7	10
146	Low Voltage Operation of High-κ HfO ₂ /TiO ₂ /Al ₂ O ₃ Single Quantum Well for Nanoscale Flash Memory Device Applications. Japanese Journal of Applied Physics, 2008, 47, 1818.	1.5	10
147	Thermal cycling induced stress–assisted sigma phase formation in super duplex stainless steel. Materials and Design, 2019, 182, 108003.	7.0	10
148	Nano-structure study of ZnO thin films on sapphire grown with different temperature conditions. Journal of Crystal Growth, 2006, 293, 344-350.	1.5	9
149	CVD growth of large-area InS atomic layers and device applications. Nanoscale, 2020, 12, 9366-9374.	5.6	9
150	Determination of thickness and lattice distortion for the individual layer of strained Al0.14Ga0.86Nâ^•GaN superlattice by high-angle annular dark-field scanning transmission electron microscopy. Applied Physics Letters, 2005, 87, 031914.	3.3	8
151	Effects of dynamic impact on mechanical properties and microstructure of special stainless steel weldments. Materials Chemistry and Physics, 2008, 111, 172-179.	4.0	8
152	Physical and Memory Characteristics of Atomic-Layer-Deposited High-κ Hafnium–Aluminum-Oxide Nanocrystal Capacitors with Iridium-Oxide Metal Gate. Japanese Journal of Applied Physics, 2009, 48, 05DF02.	1.5	8
153	Stimulated Emission in Highly (0001)-Oriented ZnO Films Grown by Atomic Layer Deposition on the Amorphous Glass Substrates. Journal of the Electrochemical Society, 2010, 157, H879.	2.9	8
154	Fatigue behavior and microstructural characteristics of a duplex stainless steel weld metal under vibration-assisted welding. Materials Science & Engineering A: Structural Materials: Properties, Microstructure and Processing, 2018, 721, 319-327.	5.6	8
155	Understanding Mechanical Properties of Nano-Grained Bainitic Steels from Multiscale Structural Analysis. Metals, 2019, 9, 426.	2.3	8
156	Hierarchical nanotwins in Fe27Co24Ni23Cr26 high-entropy alloy subjected to high strain-rate Hopkinson bar deformation. Materials Characterization, 2022, 185, 111737.	4.4	8
157	Acicular ferrite transformation in deformed austenite of an alloy-steel weld metal. Journal of Materials Science, 1995, 30, 5036-5041.	3.7	7
158	Cross-sectional transmission electron microscopy of ultra-fine wires of AISI 316L stainless steel. Philosophical Magazine, 2006, 86, 237-251.	1.6	7
159	Structural analysis of strained p-type AlGaNâ^•GaN superlattice. Journal of Applied Physics, 2007, 101, 023521.	2.5	7
160	Effect of Retained Austenite on GPM A30 High-Speed Steel. Journal of Materials Engineering and Performance, 2007, 16, 500-507.	2.5	7
161	In-situ transmission electron microscopy investigation of compressive deformation in interphase-precipitatedÂcarbide-strengthened α-iron single-crystal nanopillars. Materials Science & Engineering A: Structural Materials: Properties, Microstructure and Processing, 2019, 746, 406-415.	5.6	7
162	Microstructures of Heat-Affected Zone in Niobium Containing Steels. Materials Transactions, JIM, 1999, 40, 199-208.	0.9	6

#	Article	IF	CITATIONS
163	High-Resolution Scanning Electron Microscopy Observation of GaN/AlGaN Strained-Layer Superstructures in GaN-Based Violet Laser Diodes. Japanese Journal of Applied Physics, 2004, 43, 968-969.	1.5	6
164	Amplified Spontaneous Emission From ZnO in n-ZnO/p-GaN Heterojunction Light-Emitting Diodes With an External-Feedback Reflector. IEEE Photonics Technology Letters, 2010, 22, 248-250.	2.5	6
165	Temperature-Dependent Physical and Memory Characteristics of Atomic-Layer-Deposited <mml:math xmlns:mml="http://www.w3.org/1998/Math/MathML"><mml:mrow><mml:msub><mml:mrow><mml:mtext>RuO Nanocrystal Capacitors. Journal of Nanomaterials, 2011, 2011, 1-12.</mml:mtext></mml:mrow></mml:msub></mml:mrow></mml:math 		ex&>
166	Detection of pH and Enzyme-Free H2O2 Sensing Mechanism by Using GdO x Membrane in Electrolyte-Insulator-Semiconductor Structure. Nanoscale Research Letters, 2016, 11, 434.	5.7	6
167	Investigation of photoluminescence dynamics in InGaN/GaN multiple quantum wells. Materials Letters, 2016, 173, 170-173.	2.6	6
168	Modeling of Precipitation Hardening during Coiling of Nb–Mo Steels. Metals, 2018, 8, 758.	2.3	6
169	Size effect and strain induced double twin by nanoindentation in DSS weld metal of vibration-assisted GTAW. Materials Chemistry and Physics, 2018, 219, 40-50.	4.0	6
170	The coexistence of acicular ferrite and bainite in an alloy-steel weld metal. Journal of Materials Science Letters, 1992, 11, 1145-1146.	0.5	5
171	The influence of WidmanstÃ t ten ferrite on yielding behavior of Nb-containing reinforcing steel bars. Scripta Materialia, 2012, 67, 431-434.	5.2	5
172	Investigation of idiomorphic ferrite and allotriomorphic ferrite using electron backscatter diffraction technique. Materials Science and Technology, 2017, 33, 537-545.	1.6	5
173	Intrinsic twin boundary of ÎMgZn2 precipitates in the AA7050 aluminium alloy. Procedia Manufacturing, 2019, 37, 201-206.	1.9	5
174	Verification of the ability of Cu to dissolve in BCC δ in a δ-γ Solid Solution above 1200 °C and boosting δ nano-hardness in Cu-containing PHSS. Scripta Materialia, 2022, 211, 114505.	5.2	5
175	Microstructural evolution of simulated heat affected zone in ASTM A533 type B steel plates. Science and Technology of Welding and Joining, 1997, 2, 119-127.	3.1	4
176	Study of InGaN Multiple Quantum Dots by Metal Organic Chemical Vapor Deposition. Japanese Journal of Applied Physics, 2006, 45, 3560-3563.	1.5	4
177	Observation of ultrahigh density InGaN quantum dots. Journal of Applied Physics, 2007, 102, 013521.	2.5	4
178	The variation of beta phase morphology after creep and negative creep for duplex titanium alloys. Journal of Materials Science, 2009, 44, 408-413.	3.7	4
179	Temperature-dependent photoluminescence of arsenic-doped Si nanocrystals. Journal of Luminescence, 2010, 130, 1485-1488.	3.1	4
180	Investigation on optical and electrical properties of ZnO sandwich structure with metal interlayer. Japanese Journal of Applied Physics, 2014, 53, 05FF05.	1.5	4

#	Article	IF	CITATIONS
181	Structural investigation of Ru/Pt nanocomposite films prepared by plasma-enhanced atomic layer depositions. Micron, 2015, 74, 8-14.	2.2	4
182	Severe deformation of nanostructured bainitic steel. Procedia Engineering, 2017, 207, 1862-1867.	1.2	4
183	Dielectric properties and reliability enhancement of atomic layer deposited thin films by <i>in situ</i> atomic layer substrate biasing. Journal of Materials Chemistry C, 2020, 8, 13025-13032.	5.5	4
184	Formation of austenite from a mixture of bainitic ferrite and austenite. Materials Chemistry and Physics, 1993, 35, 168-175.	4.0	3
185	Inducement of bainite and carbide transformation from retained austenite based on a high strain rate. Scripta Materialia, 2010, 62, 372-375.	5.2	3
186	Particle Size and Morphology of Iridium Oxide Nanocrystals in Non-Volatile Memory Device. Materials Transactions, 2011, 52, 331-335.	1.2	3
187	STRUCTURAL INVESTIGATION OF n- ZnO /p- GaN ULTRAVIOLET LIGHT-EMITTING DIODES GROWN BY ATOMIC LAYER DEPOSITION. Functional Materials Letters, 2011, 04, 221-224.	1.2	3
188	Twinned formation in weld metal of titanium bearing nano precipitated high strength steel. Materials Chemistry and Physics, 2012, 136, 1103-1108.	4.0	3
189	Blue-shifted stimulated emission from ZnO films deposited on SiO2 by atomic layer deposition. Materials Chemistry and Physics, 2012, 135, 88-93.	4.0	3
190	Investigation of the microstructure and toughness of 550â€MPa grade pipeline after the hot-bending process. Materials Science and Technology, 2016, 32, 664-674.	1.6	3
191	Microstructure Characterization of Massive Ferrite in Laser-Weldments of Interstitial-Free Steels. Metals, 2020, 10, 898.	2.3	3
192	Large Delta T Thermal Cycling Induced Stress Accelerates Equilibrium and Transformation in Super DSS. Crystals, 2020, 10, 962.	2.2	3
193	Characteristics of Flakes Stacked Cr2N with Many Domains in Super Duplex Stainless Steel. Crystals, 2020, 10, 965.	2.2	3
194	Low-Temperature Physical Adsorption for the Nucleation of Sub-10 nm Al2O3 Gate Stack on Top-Gated WS2 Transistors. ACS Applied Electronic Materials, 2020, 2, 1289-1294.	4.3	3
195	Electron microscopy investigations of V defects in multiple InGaN/GaN quantum wells and InGaN quantum dots. Journal of Microscopy, 2010, 237, 275-281.	1.8	2
196	Structural and Photoluminescence Properties of ZnO Films Grown on 6H-SiC Substrates by Low-Temperature Atomic Layer Deposition. Journal of the Electrochemical Society, 2011, 158, H1213.	2.9	2
197	Unipolar Resistive Switching Memory Characteristics Using IrOx/Al2O3/SiO2/p-Si MIS Structure. ECS Transactions, 2012, 45, 345-348.	O.5	2
198	Tunable Optical and Structural Properties of Mg <i>_x</i> Zn _{1â^'<i>x</i>} O Films Prepared by In Situ Atomic Layer Doping Technique. ECS Journal of Solid State Science and Technology, 2013, 2, P31-P35.	1.8	2

#	Article	IF	CITATIONS
199	Impact of AlO <inf>x</inf> interfacial layer and switching mechanism in W/AlO <inf>x</inf> /TaO <inf>x</inf> /TiN RRAMs. , 2014, , .		2
200	Investigation of the Microstructure, Porosity, Adhesion, and Optical Properties of a WO ₃ Film Fabricated Using an E-Beam System With Ion Beam-Assisted Deposition. IEEE Transactions on Magnetics, 2014, 50, 1-4.	2.1	2
201	Impact of Intercritical Annealing on Retained Austenite and Toughness of a 460 MPa Grade Multiphase Heavy Gauge Plate Steel. Steel Research International, 2018, 89, 1800006.	1.8	2
202	Microstructural Characterization and Mechanical Properties of Duplex and Super Austenitic Stainless Steels under Dynamic Impact Deformation. Journal of Materials Engineering and Performance, 2021, 30, 8169.	2.5	2
203	Microstructural variation in fatigued interphase arrayed nano-precipitated Ti-microalloyed steel. Journal of Materials Research and Technology, 2021, 15, 2393-2404.	5.8	2
204	Decomposition of Retained Austenite in a High-Speed Steel GPM A30. Journal of Materials Engineering and Performance, 2007, 16, 102-108.	2.5	1
205	NANOSTRUCTURAL ANALYSIS OF A GaN-BASED VIOLET LASER DIODE. Surface Review and Letters, 2008, 15, 189-193.	1.1	1
206	The Structure and Ultraviolet Electroluminescence of n-ZnO-SiO2-ZnO Nanocomposite/p-GaN Heterojunction LED. ECS Transactions, 2010, 33, 267-275.	0.5	1
207	Study on sandwich structure of the transparent conducting oxide films prepared by electron beam evaporation at room temperature. , 2011, , .		1
208	The application of convergent beam electron diffraction (CBED) analysis on transformationâ€induced plasticity (TRIP) steels. Microscopy Research and Technique, 2019, 82, 4-11.	2.2	1
209	Influence of High Indium Composition InGaN on Lattice Matched ZnO Sacrificial Substrates. Journal of Light and Visual Environment, 2008, 32, 143-147.	0.2	1
210	Metalorganic chemical vapor deposition and structural/optical characteristics of InGaN/GaN multiple quantum wells grown on sapphire for light emitting diode application. , 2005, , .		0
211	Photoluminescence dynamics and structural investigation of InGaN/GaN multiple quantum well light emitting diodes grown by metalorganic chemical vapor deposition. , 2007, , .		0
212	STRUCTURAL AND OPTICAL PROPERTIES OF InGaN / GaN MULTIPLE QUANTUM WELL LIGHT EMITTING DIODES GROWN BY METALORGANIC CHEMICAL VAPOR DEPOSITION. , 2008, , 57-88.		0
213	Optical and structural properties of dual wavelength InGaN/GaN multiple quantum well light emitting diodes. , 2008, , .		0
214	Optical properties and material studies of InGaN/GaN multi-quantum well light emitting diode wafers with different structures. Proceedings of SPIE, 2009, , .	0.8	0
215	Materials science and engineering at National Taiwan University. International Heat Treatment and Surface Engineering, 2010, 4, 48-49.	0.2	0
216	Density and Grain Size of the IrOx Metal Nanocrystals in n-Si/SiO2/Al2O3/IrOx/Al2O3 Memory Capacitors. ECS Transactions, 2010, 33, 333-337.	0.5	0

#	Article	IF	CITATIONS
217	Characteristics of ALD High-k HfAlOx Nanocrystals in Memory Capacitors Annealed at High Temperatures. ECS Transactions, 2010, 33, 347-353.	0.5	0
218	Effects of Iridium Oxide Thickness and Post Annealing Temperature on the Size and Density of Core-Shell IrOx-Based Nanocrystals of a Nonvolatile Memory Device. ECS Transactions, 2011, 41, 115-119.	0.5	0
219	Low current cross-point memory using gadolinium-oxide switching material. , 2014, , .		0
220	B22-P-09The misorientation change in lenticular martensite by Electron Backscattered Diffraction and Convergent Beam Kikuchi Line Diffraction Pattern. Microscopy (Oxford, England), 2015, 64, i107.1-i107.	1.5	0
221	B11-P-11The effect of aging on the phase transformation of AA7050 aluminum alloys. Microscopy (Oxford, England), 2015, 64, i83.2-i83.	1.5	0
222	Structure and electrical property changes of ZnO:Al films, prepared by radio frequency magnetron sputtering, by thermal annealing. Microscopy and Microanalysis, 2015, 21, 1797-1798.	0.4	0
223	Structure of Ru/Pt Nanocomposite Films Fabricated by Plasma-Enhanced Atomic Layer Depositions. Microscopy and Microanalysis, 2015, 21, 1931-1932.	0.4	0
224	B12-O-18Insight into the Deformation Behavior of Spinodal Nanostructured δ-Ferrite in a 2205 Duplex Stainless Steel. Microscopy (Oxford, England), 2015, 64, i27.2-i27.	1.5	0
225	Twin relationship in between the variant-pair of η precipitates in the Al-Zn-Mg-Cu aluminium alloy. MATEC Web of Conferences, 2020, 326, 01002.	0.2	0